Self-assisted membrane-penetrating helical polypeptides mediate anti-inflammatory RNAi against myocardial ischemic reperfusion (IR) injury

Liang, Qiujun; Li, Fangfang; Liu, Yongjuan; Liu, Yong; Lan, Min; Wu, Songhua; Wu, Xuejie; Ji, Yong; Zhang, Rujing; Yin, Lichen

Published in:
Biomaterials Science

DOI:
10.1039/c9bm00719a

Publication date:
2019

Biomaterials Science

PAPER

View Article Online
View Journal | View Issue

Cite this: *Biomater. Sci.*, 2019, **7**, 3717

Self-assisted membrane-penetrating helical polypeptides mediate anti-inflammatory RNAi against myocardial ischemic reperfusion (IR) injury†

Qiujun Liang,[a] Fangfang Li,[a] Yongjuan Li,[a] Yong Liu, *[b] Min Lan,[a] Songhua Wu,[c] Xuejie Wu,[c] Yong Ji,*[d] Rujing Zhang[e] and Lichen Yin *[a]

Received 8th May 2019,
Accepted 27th May 2019

DOI: 10.1039/c9bm00719a

rsc.li/biomaterials-science

Anti-inflammatory RNA interference (RNAi) provides a promising paradigm for the treatment of myocardial ischemia reperfusion (IR) injury. To overcome the membrane barriers against intracardial siRNA delivery, various guanidinated helical polypeptides with potent and aromaticity-assisted membrane activities were herein developed and used for the delivery of siRNA against RAGE (siRAGE), a critical regulator of the pro-inflammatory cascade. Aromatic modification of the polypeptide led to notably enhanced transmembrane siRNA delivery efficiencies, and more importantly, allowed more siRNA cargoes to get internalized *via* non-endocytosis, an effective pathway toward gene transfection. Subsequently, benzyl-modified polypeptide (P-Ben) was identified as the top-performing material with the highest RAGE silencing efficiency yet lowest cytotoxicity in H9C2 cells. Intracardial injection of the P-Ben/siRAGE polyplexes at 150 μg siRNA per kg led to remarkable RAGE knockdown by ~85%, thereby attenuating the inflammatory cytokine release and reducing the cardiomyocyte apoptosis as well as myocardium fibrosis to recover the cardiac function after IR injury. This study therefore provides an effective strategy for the design of membrane-penetrating gene delivery materials, and may provide a promising addition to the anti-inflammatory treatment of myocardial IR injury.

Introduction

Myocardial infarction (MI) is a major cause of cardiac dysfunction with high morbidity and mortality.[1–3] During the healing process post myocardial ischemia reperfusion (IR) injury, the overwhelming inflammation fueled by continuous up-regulation of pro-inflammatory cytokines can exacerbate tissue damage, thus contributing to adverse cardiac remodeling and non-contractile collagen deposition that ultimately impedes cardiac repair.[4–9] Therefore, inhibition of the unbridled inflammatory cascades has provided a promising modality for the treatment of myocardial IR injury.[10–13] In the past decades, various types of anti-inflammatory drugs, such as non-steroidal drugs, inhibins, angiotensin converting enzyme inhibitors, and anticoagulants, have been utilized for the treatment of myocardial IR injury.[14,15] Although these chemotherapeutics have shown some success, multiple potential side effects, including edema at lower extremity, dizziness, nausea, insomnia, and depression, may cause great discomfort for patients. Recently, chemokine-targeted antibody therapy has received great attention due to its favorable anti-inflammation effect, however, the high cost and immunogenecity of antibodies still pose great challenges against their wide applications in the clinical setting.[16,17]

RNA interference (RNAi) mediated by small interfering RNA (siRNA) has recently emerged as a potent treatment paradigm for many diseases, because of its capability to inhibit gene expression *via* sequence-specific degradation of targeted mRNA at high efficiency and specificity.[18–25] Various inflam-

[a]*Institute of Functional Nano and Soft Materials (FUNSOM), Jiangsu Key Laboratory for Carbon-Based Functional Materials and Devices, Collaborative Innovation Center of Suzhou Nano Science & Technology, Soochow University, Suzhou 215123, China. E-mail: lcyin@suda.edu.cn*
[b]*Department of Biomedical Engineering, University of Groningen and University Medical Center Groningen, Antonius Deusinglaan 1, 9713 AV Groningen, The Netherlands. E-mail: y.liu@umcg.nl*
[c]*Department of Cardiothoracic Surgery, the Second Affiliated Hospital of Soochow University, Suzhou 215004, China*
[d]*Department of Cardiothoracic Surgery, Wuxi People's Hospital Affiliated to Nanjing Medical University, Wuxi 214023, China. E-mail: jiyongmyp@163.com*
[e]*Department of Micro- and Nanotechnology, DTU Nanotech, Technical University of Denmark, 2800 Kgs. Lyngby, Denmark*

†Electronic supplementary information (ESI) available: Detailed description of instrumentation, ^{1}H NMR spectra, and additional experimental results. See DOI: 10.1039/c9bm00719a

matory factors, such as transforming growth factor β (TGF-β), Src homology region 2 domain-containing tyrosine phosphatase-1 (SHP-1), receptor for advanced glycation end products (RAGE), and CD47 can thus be down-regulated *via* RNAi to treat IR injury.[26–28] Among them, RAGE is a pattern-recognition receptor for various ligands that accumulate at the inflammation site, including s100/calgranulin and high mobility group 1 (HMGB 1).[27,29] The specific interactions between RAGE and its ligands could regulate inflammatory reactions by activating several signaling cascades, such as the JAK/STAT pathway, ERK1/2 MAP kinases, and SAPK/JNK MAP kinases pathways, consequently leading to NF-κB activation.[30–32] Recent studies have also demonstrated RAGE as a critical regulator during the pro-inflammatory and pro-apoptotic cascades after myocardial IR injury.[33,34] Therefore, RNAi against RAGE expression could potentially impart anti-inflammatory effect to treat myocardial IR injury.[31,34]

To realize anti-inflammatory RNAi in cardiac tissues/cells, an efficient and safe siRNA delivery vehicle is highly critical. While cationic polymers that can condense nucleic acids into polyplexes have been widely utilized for siRNA delivery,[35–37] they often suffer from low delivery efficiency in the myocardium due to the various biological barriers, especially posed by the cellular membranes and endolysosomal membranes.[38,39] Particularly, the cell membrane prevents the internalization of polyplexes into cardiac cells especially in the case of compact cardiac ventricles muscle structure in myocardium.[40] The slow division rate and intrinsic poor internalization capability of myocytes further impede the polyplexes from effective transfection.[41] Moreover, the cationic polyplexes are often internalized by target cells *via* endocytosis, which will subsequently experience severe endosomal/lysosomal entrapment to prevent efficient delivery of siRNA cargoes into the cytoplasm.

To overcome these biological membrane barriers, we recently developed α-helical cationic polypeptides with potent membrane-penetrating properties, which can thus mediate effective trans-membrane nucleic acid delivery.[42–46] The helical polypeptide with stiff, rod-like structure can mediate "pore formation" on cell membranes, a mechanism that is effective toward trans-membrane delivery but also causes irreversible damage to the cell membranes.[47] Additionally, only part of the polypeptide-based polyplexes enters the cells *via* the non-endocytic pathway, while the remaining proportion is still internalized *via* endocytosis, which will be entrapped by endolysosomes to diminish the transfection availability of the gene cargo.

With the attempt to potentiate the trans-membrane siRNA delivery efficiency and reduce the cytotoxicity of the helical polypeptides, various aromatically modified helical polypeptides were herein developed to mediate anti-inflammatory RNAi in IR-injured myocardium. The aromatic domains with flat-rigid shapes and π-electronic structures render strong interactions with biological membranes,[26] and we thus reason the incorporation of aromaticity could enhance the trans-membrane delivery efficiency of siRNA in myocytes. Additionally, aromatic groups can contribute to a direct trans-

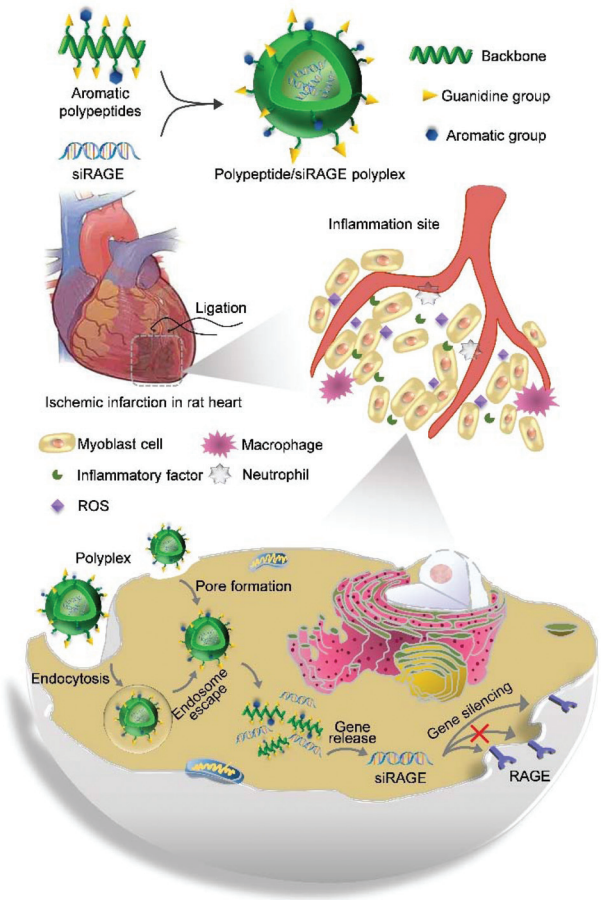

Scheme 1 Schematic illustration of aromaticity-assisted RAGE siRNA delivery mediated by the membrane-penetrating helical polypeptide toward anti-inflammatory treatment of myocardial IR injury.

duction mechanism during cell penetration, a non-endocytic and non-pore formation mechanism that would ideally reduce the pore formation-associated materials toxicity while without compromising the membrane activity. As such, polypeptide was synthesized *via* ring-opening polymerization (ROP) of *N*-carboxyanhydride (NCA), into which guanidine as the charged group and various aromatic groups (benzyl, naphthyl, biphenyl, anthryl, and pyrenyl) were incorporated on the side-chain terminals *via* the click reaction. siRNA against RAGE (siRAGE) was delivered by the aromatic, helical polypeptides to mediate anti-inflammatory treatment against myocardial IR injury both *in vitro* and *in vivo*, and the aromaticity-assisted membrane-penetrating mechanism was systemically investigated (Scheme 1).

Experimental

Materials, cells, and animals

All chemicals and solvents used were purchased from Energy Chemical (Shanghai, China) unless otherwise indicated. Polyethylenimine (PEI, branched, MW = 25 kDa) was pur-

chased from Sigma-Aldrich (St Louis, USA). γ-Propargyl-L-glutamate-based *N*-carboxyanhydride (PLG-NCA) was synthesized as reported before.[48] RAGE siRNA (siRAGE), scrambled siRNA (siScr), and primers of RAGE and GAPDH were purchased from GenePharma (Shanghai, China), and their sequences were shown in Tables S1 and S2.†

H9C2 cells (rat heart myoblast) were purchased from Bioleaf (Shanghai, China) and were cultured in DMEM containing 1% nonessential amino acids, 1% L-glutamine, and 10% fetal bovine serum (FBS) in a humidified atmosphere of 95% O_2 and 5% CO_2.

Male Sprague-Dawley (SD) rats (200–250 g, 8–10 weeks) were purchased from Shanghai Slaccas Experimental Animal Co., Ltd (Shanghai, China) and housed in a clean room at 25 °C with 12:12 h light/dark cycle. All animal procedures were performed in strict accordance with the NIH guidelines for the care and use of laboratory animals (NIH Publication 85-23 Rev. 1985) and experiments were approved by the Animal Ethics Committee of Soochow University.

Synthesis of azido guanidines

1,6-Dibromopentane and NaN_3 were mixed in dimethylformamide (DMF, 25 mL) and stirred for 24 h at 60 °C. DI water (150 mL) was added, and the reaction mixture was extracted with ether. The organic phase was dried with Na_2SO_4, and the product 1,6-diazidohexane was obtained after removal of the solvent under vacuum (yield 90%).

1,6-Diazidohexane (33 mmol) was dissolved in ether (20 mL) and ethyl acetate (20 mL), and 5% HCl was added (45 mL). Triphenylphosphine (34 mmol) was then added into the solution in small portions over 1 h at 0 °C. After the reaction mixture was stirred at room temperature for 24 h, HCl (1 M, 40 mL) was added. The aqueous layer was washed with dichlomethane (DCM, 30 mL) for three times and further basified using NaOH solution (1 M) until pH reached 12. After extraction with DCM (30 mL) for four times, the organic phase was dried over Na_2SO_4. The product 6-azido-1-hexylamine was obtained as light yellow oil after removal of the solvent under vacuum (yield 38%).

6-Azido-1-hexylamine (2.13 g), *H*-pyrazole-1-carboxamidine hydrochloride (2.21 g), and *N*,*N*-diisopropylethylamine (DIEA, 2.61 mL) were dissolved in dry DMF (18 mL). The mixture was stirred at room temperature overnight. Ether (150 mL) was added to the reaction mixture to precipitate the crude product, which was then washed with ether and dried under vacuum to obtain 6-azido-1-hexylguanidine (N_3-HG, yield 61%).

Synthesis of azido phenyls

Benzyl chloride (2 mmol) and NaN_3 (3 mmol) were dissolved in a mixture of acetone (35 mL) and DI water (10 mL), and the reaction mixture was refluxed for 24 h at 50 °C. After removal of the solvent, the residue was dissolved in DCM (100 mL), washed with DI water (30 mL) for three times, and dried over anhydrous $MgSO_4$. The crude product was purified by silica gel column chromatography (DCM/MeOH = 1/1, v/v) to obtain benzyl azide (Ben-N_3, yield 62%).

Naphthylazide (Naph-N_3, yield 81%), 4-(azidomethyl)-1,1′-biphenyl (Biph-N_3, yield 73%), 9-(azidomethyl) anthracene (Anth-N_3, yield 51%), and 1-(azidomethyl) pyrene (Pyre-N_3, yield 78%) were similarly synthesized starting from 1-(chloromethyl) naphthalene (Naph-Cl), 4-(chloromethyl)-1,1′-biphenyl (Biph-Cl), 9-(chloromethyl) anthracene (Anth-Cl), and 1-(chloromethyl) pyrene (Pyre-Cl), respectively. The ^{1}H NMR characterization of azido-phenyls was shown in Table S3.†

Synthesis of poly(γ-propargyl-L-glutamate) (PPLG)

PPLG was polymerized from PLG-NCA initiated by hexamethyldisilazane (HMDS). In a glovebox, HMDS dissolved in DMF (28 μL, 0.1 mol L^{-1}, M/I = 100) and TBD dissolved in DMF (56 μL, 0.01 mol L^{-1}) were added to a DMF solution of PLG-NCA (60 mg, 0.28 mmol, 1 mL), and the reaction mixture was stirred for 48 h at room temperature. The solution was then precipitated using cold methanol and PPLG was obtained as yellow solid (yield 38%).

Synthesis of guanidine and aromatic group-modified polypeptides

PPLG was with aromatic and guanidine groups *via* the "click" reaction in a glove box. Briefly, PPLG polymer (0.06 mmol, 10 mg), *N*,*N*,*N*,*N*,*N*″-pentamethyldiethylenetriamine (PMDETA, 0.32 mmol), N_3-HG (85 mol%, 0.102 mmol) and small molecular azides with various aromatic groups (15 mol%, 0.018 mmol) were dissolved in DMF (2 mL), and then CuBr (0.06 mmol, 8.78 mg) was added. The solution was stirred for 48 h at room temperature, and HCl (1 M, 1 mL) was then added. The mixture was dialyzed against DI water (MWCO = 3.5 kDa) for 3 days, and lyophilized to obtain the final polypeptides, P-Ben (yield 30%), P-Biph (yield 27%), P-Nath (yield 29%), P-Anth (yield 27%), and P-Pyre (yield 23%) that were synthesized from Ben-N_3, Naph-N_3, Biph-N_3, Anth-N_3, and Pyre-N_3, respectively. The homopolypeptide, P-Homo, was similarly synthesized from PPLG and N_3-HG (yield 37%). The ^{1}H NMR characterization of all polypeptides was shown in Table S3.†

Preparation and characterization of polypeptide/siRNA polyplexes

Polypeptide solution (1 mg mL^{-1} in DEPC water) was mixed with siRNA solution (1 mg mL^{-1} in DEPC water) at various polymer/siRNA weight ratios (1, 5, 10, 15, and 20). The mixture was vortexed for 5 s and incubated at RT for 30 min to form polyplexes. To evaluate the siRNA condensation, the polyplexes were subjected to electrophoresis in 2% agarose gel at 90 mV for 20 min to observe the siRNA migration (GE Amersham Imager 600, Boston, USA). The quantitative evaluation of siRNA condensation level was further measured using the ethidium bromide (EB) exclusion assay. Briefly, EB was added to siRNA solution at the siRNA/EB ratio of 10 : 1 (w/w), and the mixture was incubated at room temperature for 1 h. Polypeptide was dissolved in water at 1 mg mL^{-1} and was added to siRNA/EB mixture at various weight ratios, vortexed for 30 s, and incubated at room temperature for 30 min before measurement of the fluorescence intensity (λ_{ex} =

510 nm, λ_{em} = 590 nm). The siRNA condensation efficiency (%) was defined as follows:

$$\text{siRNA condensation efficiency}\,(\%) = \left(1 - \frac{F - F_{EB}}{F_0 - F_{EB}}\right) \times 100$$

where F_{EB} represents the fluorescence intensity of pure EB solution, F_0 represents siRNA/EB solution without any polypeptide, and F represents siRNA/EB solution with different polypeptides.

Size and zeta potential of freshly formed polyplexes were measured by dynamic laser scattering (DLS, Zetasizer Nano-ZS, Malvern).

In vitro transfection in H9C2 cells

H9C2 cells were seeded on a 6-well plate at 5×10^5 cells per well and cultured for 24 h under normoxic condition (20% O_2, 5% CO_2, and 75% N_2). Cells were transfected with polymer/siRAGE polyplexes (1 μg mL^{-1} siRNA) in serum-free DMEM for 4 h, followed by incubation in fresh serum-containing medium for 20 h. Cells were further incubated under hypoxic condition (1% O_2, 5% CO_2, and 95% N_2) for another 6 h,[27] and the gene silencing efficiency was determined by real-time PCR. Total RNA was isolated from H9C2 cells using the Total RNA Isolation Reagent (Biosharp, Shanghai, China), and 2 μg of RNA was subjected to reverse transcription using the PrimeSccript RT reagent Kit (Takara Bio, Shiga, Japan) to generate cDNA. Real-time PCR analysis was then carried out using SYBR Premix Ex Taq (Takara Bio, Shiga, Japan) on a CFX Connect Real-Time System (Bio-Rad, USA). RAGE mRNA of each sample was quantified by the comparative Ct method and normalized to GAPDH in the same run. The gene silencing efficacy was represented as the percentage of RAGE mRNA level of control cells without polyplexes treatment.

Cytotoxicity

H9C2 cells were seeded on a 96-well plate at 1×10^4 cells per well and cultured at 37 °C for 24 h. The medium was replaced by serum-free DMEM (90 μL per well), into which polymer/siRNA polyplexes at various weight ratios were added (1 μg mL^{-1} siRNA). After incubation for 4 h, cells were further cultured for another 20 h in fresh serum-containing DMEM before cell viability assessment using the MTT assay. Results were represented as percentage viability of control cells that did not receive polyplexes treatment.

Cell uptake and intracellular kinetics

H9C2 cells were seeded on a 24-well plate at 1×10^4 cells per well and cultured for 24 h. The medium was replaced by opti-MEM (500 μL per well) and various polymer/FAM-siRNA polyplexes were added (w/w = 15 for polypeptide, w/w = 2.5 for PEI, 1 μg mL^{-1} siRNA). After treatment for 4 h, cells were washed with heparin-containing PBS for three times, and subjected to flow cytometric analysis. Cells without polyplexes treatment served as the blank.

To determine the internalization mechanism of polyplexes, the cellular uptake assay was conducted at 4 °C or in the presence of various endocytic inhibitors. Cells were treated with different polyplexes (w/w = 15, 2 μg mL^{-1} siRNA) for 4 h at 4 °C. Otherwise, cells were pretreated with inhibitors, including genistein (100 μg mL^{-1}), methyl-β-cyclodextrin (mβCD, 5 mM), chlorpromazine (10 μg mL^{-1}), or wortmannin (10 μg mL^{-1}) for 30 min followed by incubation with polyplexes for 4 h at 37 °C. The results were expressed as percentage uptake level of control cells which were treated with polyplexes in the absence of endocytic inhibitors for 4 h at 37 °C.

To evaluate the "pore formation" ability of polypeptides, H9C2 cells seeded in a 96-well plate (~80% confluence) were incubated with fluorescein-tris(hydroxymethyl) methanethiourea (FITC-Tris, 10 μg mL^{-1}), a membrane-impermeable dye, and polypeptide (20 μg mL^{-1}) for 2 h. Cells were then washed with PBS containing heparin for three times, and lysed using the RIPA lysis buffer (100 μL per well). The cellular uptake level of FITC-Tris was measured by the spectrofluorimetry (λ_{ex} = 495 nm, λ_{em} = 519 nm), and the protein content was monitored by the BCA kit. The result was represented as μg FITC-Tris per mg protein.

To explore the endosomal escape of polyplexes, H9C2 cells were seeded on coverslips (1.5 × 1.5 cm) in a 24-well plate at 5×10^3 cells per well and cultured at 37 °C for 24 h. After treatment with polypeptide/FAM-siRNA polyplexes (w/w = 15, 2 μg mL^{-1} siRNA) for 4 h in serum-free DMEM, cells were washed with cold PBS containing heparin (20 IU mL^{-1}) for three times, stained with Lysotracker Red (200 nM), fixed with 4% paraformaldehyde, and then stained with DAPI (5 μg mL^{-1}) before confocal laser scanning microscopy (CLSM, TCS SP5, Leica, Germany) observation. The colocalization ratio between green (FAM-siRNA) and red (Lysotracker Red-stained endolysosomes) fluorescence in 20 individual cells was calculated using the ImageJ software.

Establishment of rat myocardial infarction model

Rats were anesthetized *via* intraperitoneal injection of pentobarbital sodium (80 mg kg^{-1}), and were intubated and ventilated using a rodent ventilator with tidal volume of 2 mL per 100 g. Heart of the rat was exposed through a 2 cm incision at the left intercostal space, and the left anterior descending (LAD) artery was ligated using a 6–0 prolene suture for 40 min. Ischemia was monitored by visual inspection of whitening in the myocardium apex distal to the ligation site.[27] After loosening of the suture for 10 min to allow reperfusion, saline or polymer/siRNA polyplexes (150 μg siRNA per kg), including PEI/siRAGE (w/w = 5), P-Ben/siScr (w/w = 20), P-Ben/siRAGE (w/w = 20), and P-Homo/siRAGE (w/w = 20) polyplexes, were injected into the myocardium below the LAD site (50 μL per rat, four rats per group). Then the chest was closed after sucking out the air from the chest cavity through a rubber tube needle. As a normal control, the same surgical procedure was carried out in rats except LAD ligation in the artery. The mRNA and protein levels of RAGE in the ischemic myocardium were measured at 24 h post IR injury using real-time PCR and western blot, respectively. The expression levels of pro-inflammatory cytokines, TNF-α and IL-6, were monitored using western blot and immunostaining at 24 h post IR injury.

Cardiac function was examined by echocardiography three days after IR injury. Rats were then sacrificed, and hearts were harvested to determine the infarction size. In a parallel study, rat hearts were harvested and subjected to histological analysis one week after IR injury. For histological analysis, the collected heart samples were fixed in 10% formaldehyde for one day, embedded in paraffin, and cut into 8 μm sections before staining with different reagents. All the echocardiographic analyses and histological measurements were performed in a blinded manner.

In vivo cardiac cell uptake

To evaluate the distribution of polyplexes *in vivo*, polymer/Cy3-siRNA polyplexes were injected into rat myocardium 10 min after IR injury with naked Cy3-siRNA as the control (200 μg siRNA per kg). Four hours after injection, the hearts were harvested, washed with PBS, and embedded in OCT compound at −80 °C overnight. The tissue was cut into 10 μm section using cryostat (Leica, Germany), stained with FITC-phalloidine (50 μg mL^{-1}) for 40 min and DAPI (10 μg mL^{-1}) for 10 min at room temperature, covered by the Anti-fade Mounting Medium (Solarbio), and then observed with CLSM.

To further quantify the *in vivo* uptake level of siRNA in cardiac cells after IR injury, rats were injected with different polymer/FAM-siRNA polyplexes (200 μg siRNA per kg) or PBS at 10 min post IR injury. Rats were sacrificed after 4 h and the heart was harvested, washed by PBS, cut into pieces, and incubated with hyaluronidase and collagenase (1.5 mg mL^{-1}) at 37 °C for 1 h. The mixture was filtered with nylon mesh and the cells were centrifuged at 1500 rpm for 3 min. RBC lysis buffer (1 mL) was added and incubated for 3 min, followed by addition of DMEM containing 10% FBS (3 mL). Then the suspension was centrifuged at 1500 rpm for 3 min, washed with the FACS buffer (PBS containing 1% FBS), and finally resuspended in the FACS buffer (500 μL) followed by flow cytometric analysis to determine the cardiac cell uptake level.

In vivo RAGE silencing efficiency

Rat hearts were harvested at 24 h post IR injury, homogenized in the Total RNA Isolation Reagent, and total RNA was extracted as described above. RAGE mRNA levels were determined using real-time PCR. The RAGE protein level was monitored by western blot, and the concentration of each antibody used was as follows, primary antibodies anti-RAGE (Abcam, 1 : 1000), anti-GAPDH (Abcam, 1 : 2000), and secondary antibody goat-anti-rabbit IgG (Abcam, 1 : 1000).

In vivo anti-inflammatory effect

Rat hearts harvested at 24 h post IR injury were embedded in OCT, cut into 10 μm sections using cryostat, and fixed in acetone at 4 °C for 5 min. The sections were rinsed with 1% PBS for three times, and immunofluorescence staining was carried out through the following steps, including blocking with 5% BSA for 2 h, incubation with primary antibody at 4 °C overnight, incubation with secondary antibody for 1 h at RT, and staining with DAPI (10 μg mL^{-1}) for 10 min, before observation by CLSM. The concentration of each antibody was as follows, primary antibodies anti-TNF-α (Abcam, 1 : 100) and anti-IL-6 (Abcam, 1 : 100); secondary antibodies FITC-goat anti-rabbit IgG (1 : 50) and Cy5-goat anti-mouse IgG (1 : 50). The TNF-α protein levels in rat hearts were also determined by western blot as described above.

Infarct size and fibrosis analysis

To measure the infarct size, collected heart was cut into five sections transversely and soaked in 2,3,5-triphenyltetrazolium chloride (TTC) solution (1%) at 37 °C for 20 min without light. Then the stained samples were fixed in 10% formalin at 4 °C. The heart sections were scanned by a digital scanner (Canon, Shanghai, China) to visualize the normal area (red) and infarcted area (white). The infarct size (%) was calculated as the weight of infarcted area normalized by that of the total left ventricle. The fibrosis level in heart samples was determined by hematoxylin & eosin (H&E) and Masson's trichrome (MT) staining, followed by observation using optical microscopy. MT staining is a three-color staining method commonly used in histology, which reveals red muscles and blue collagen fibers.[49] Three sample slides were prepared per animal, and a total of five randomly picked high-power fields per slide were examined to calculate the fibrosis ratio (%) denoted as MT-stained fibrotic area (blue) normalized by the total area.

Anti-apoptotic effect

Paraffin sections of heart tissues were stained with the Colorimetric TUNEL Apoptosis Assay Kit® (Beyotime Biotechnology, China), and observed by optical microscopy. Three sample slides were prepared per animal, and a total of five randomly picked high-power fields per slide were examined to calculate the cell apoptotic ratio (%).

Echocardiographic analysis

Echocardiographic measurements were carried out on a Philips high-resolution ultrasound system by an experienced technician blinded to the experimental groups. All the measurements were averaged over three consecutive cardiac cycles, and the cardiac systolic function of rats under anesthesia was represented by two critical parameters, left ventricular ejection fraction (EF, %) and fractional shortening (FS, %).

Statistical analysis

All the experimental data was presented as the mean ± standard deviation of independent measurements ($n \geq 3$ samples per group). Statistical analysis was carried out using Student's *t*-test and differences were assessed to be significant at $^{*}p < 0.05$ and very significant at $^{**}p < 0.01$ and $^{***}p < 0.001$.

Results and discussion

Synthesis and characterization of aromatic helical polypeptides

To synthesize polypeptides with both guanidine (85 mol%) and aromatic (15 mol%) side chains, PLG-NCA bearing alkyne

group was polymerized *via* HMDS-mediated ring-opening polymerization (ROP), and the obtained PPLG was functionalized with N_3-HG and various azido phenyls on the side-chain terminals *via* the azide–alkyne Huisgen cycloaddition (so-called "click" chemistry) (Fig. 1A). HMDS allowed a controlled polymerization,[50] resulting in PPLG with desired degree of polymerization (DP = 113 at the M/I ratio of 100) and a narrow molecular weight distribution (MWD = 1.18) as determined by GPC (Fig. S1†). CD analysis showed that all the polypeptides adopted typical α-helical conformation at the helicity of 62–82%, as indicated by the characteristic minima ellipticity at 208 and 222 nm (Fig. 1B). P-Homo showed similar helicity to other copolypeptides, indicating that the introduction of aromatic groups did not significantly compromise its helical structure.

Characterization of polypeptide/siRNA polyplexes

siRNA condensation by the polypeptides was evaluated by the gel retardation assay. As shown in Fig. 2A, all the helical polypeptides could condense siRNA at the weight ratios ≥10, and similar results were obtained from the quantitative EB exclusion assay (Fig. 2B). It was noted that the aromatic polypeptides displayed slightly lower siRNA binding affinities than the homopolypeptide (P-Homo), which could be attributed to the partial loss of positive charges on polymer side chains. Furthermore, DLS measurement showed that all the polypeptides were able to condense siRNA to form polyplexes with diameters of 100–200 nm and positive surface charges at weight ratios ≥5 (Fig. S2†).

In vitro RAGE silencing efficiency

In vitro silencing of RAGE expression in H9C2 cells mediated by different polyplexes was evaluated by real-time PCR (Fig. 3). All the aromatic polypeptides except P-Pyre exhibited significantly higher gene silencing efficiencies than the homopolypeptide P-Homo, which suggested that aromatic modification contributed to the siRNA delivery efficiencies in H9C2 cells presumably due to the enhanced membrane activities of the polypeptides. Among them, P-Ben and P-Anth displayed the highest RAGE knockdown efficiencies of ~70%, significantly outperforming commercial reagent PEI.

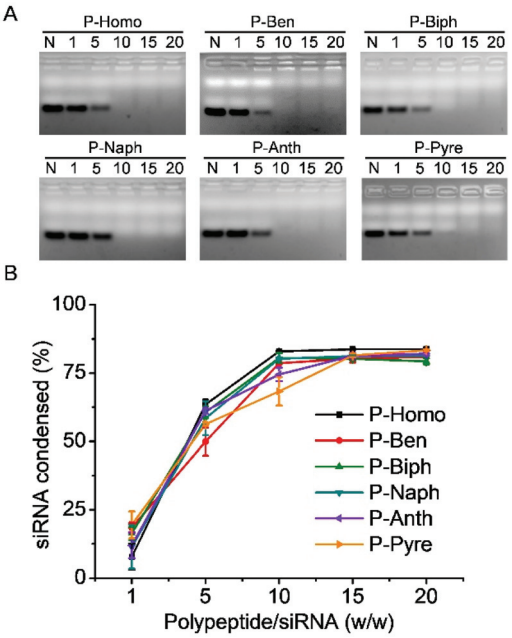

Fig. 2 siRNA condensation by polypeptides at various polypeptide/siRNA weight ratios as evaluated by the gel retardation assay (A) and EB exclusion (B). N represents naked siRNA.

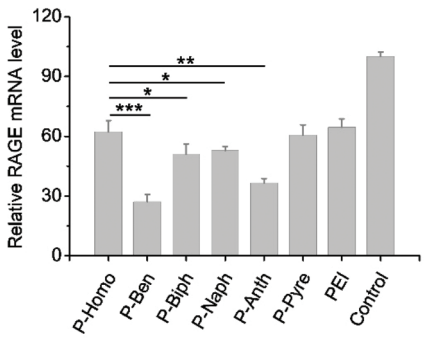

Fig. 3 Relative RAGE mRNA levels in H9C2 cells after treatment with different polymer/siRAGE polyplexes (1 μg siRNA per mL, polypeptide/siRNA = 15, PEI/siRNA = 2.5, w/w, n = 3).

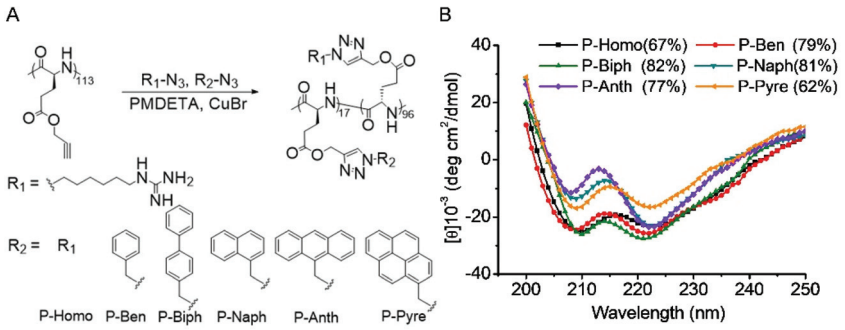

Fig. 1 (A) Synthetic route and chemical structures of aromatically modified polypeptides. (B) CD spectra of polypeptides (0.05 mg mL^{-1}) in the aqueous solution at pH 7.0. Calculated helicity of each polymer was incorporated in the parentheses.

Cytotoxicity of polyplexes

The transfection efficiency and cytotoxicity of polycations are often inversely correlated.[51] Therefore, an optimal balance between these two parameters is crucial towards the design of non-viral gene vectors. Herein, cytotoxicity of the polypeptide/siRNA polyplexes at various weight ratios was assessed by the MTT assay. As shown in Fig. 4, the cell viability decreased as the polypeptide/siRNA weight ratio increased, indicating a concentration-dependent cytotoxicity of the helical polypeptides. Compared to P-Homo, P-Ben and P-Naph displayed slightly lower cytotoxicity with cell viability of ~85% at the polypeptide/siRNA weight ratio of 15, which could be attributed to the higher cationic charge density of P-Homo that correlated to the "pore formation" mechanism.[52,53] In comparison, P-Biph, P-Anth, and P-Pyre showed stronger cytotoxicity than P-Homo. Thus, P-Ben/siRAGE polyplexes (w/w = 15) with the highest RAGE silencing efficiency yet lowest cytotoxicity were identified for the following mechanistic study and *in vivo* application.

Cell uptake and intracellular kinetics

The performance of non-viral gene delivery vectors is largely dependent on their intracellular kinetics, including cellular uptake level, internalization pathway, and endosomal escape mechanism. Flow cytometric analysis showed that, aromatic polypeptides were able to notably enhance the cellular uptake of FAM-siRNA than the homopolypeptide, significantly outperforming PEI (Fig. 5A and B). These results illustrated the pivotal role of aromatic domains in enhancing the trans-membrane siRNA delivery efficiencies of polypeptides.

The internalization pathway often dominates the intracellular fate of siRNA cargoes and ultimately the gene silencing efficiency. Most of the cationic gene vectors mediate intracellular siRNA delivery through endocytosis that often leads to endosomal/lysosomal entrapment of siRNA cargoes, which will greatly compromise the transfection efficiency unless an efficient endolysosomal escape mechanism occurred. Therefore, we investigated the internalization mechanism of polyplexes by monitoring the cellular uptake level at 4 °C when the energy-dependent endocytosis pathway was blocked. As shown in Fig. 5C, P-Homo-mediated FAM-siRNA uptake level was inhibited by 44.7% at 4 °C, while lower inhibitory rates

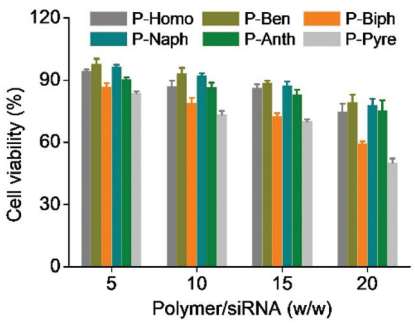

Fig. 4 Cytotoxicity of polypeptide/siRAGE polyplexes at various weight ratios toward H9C2 cells (1 μg siRNA per mL, n = 3).

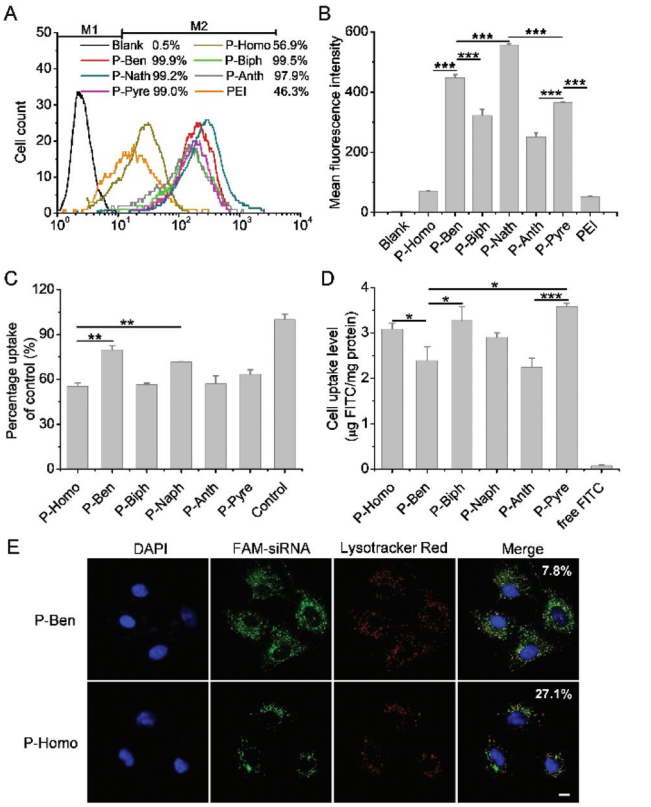

Fig. 5 Intracellular kinetics of polyplexes in H9C2 cells. (A) Flow cytometric analysis on the cell uptake of polymer/FAM-siRNA polyplexes (polypeptide/siRNA = 15, PEI/siRNA = 2.5, w/w) in H9C2 cells following incubation for 4 h at 37 °C. M1 and M2 phases represent FAM-siRNA negative and positive cells, respectively. The listed numbers are the percentage of M2 cells. (B) Mean fluorescence intensity per cell as calculated from flow cytometric analysis in (A) (n = 3). (C) Relative uptake levels of different polyplexes containing FAM-siRNA in H9C2 cells at 4 °C (n = 3). (D) The cellular uptake level of FITC-Tris (10 μg mL^{-1}) following co-incubation with polypeptides (20 μg mL^{-1}) for 2 h at 37 °C (n = 3). (E) CLSM images of cells treated with P-Ben/FAM-siRNA and P-Homo/FAM-siRNA polyplexes (w/w = 15) for 4 h. The colocalization ratios between FAM-siRNA and Lysotracker Red-stained endolysosomes were listed (n = 20). Scale bar = 10 μm.

were observed for P-Ben/siRNA polyplexes (20.3%) and P-Naph/siRNA polyplexes (28.5%), implying that the aromatic groups (Ben and Naph) in the polypeptides promoted the non-endocytic delivery of siRNA into cells. In comparison, polypeptides modified with other aromatic groups (Biph, Anth, and Pyre) showed almost the same inhibitory level as P-Homo, indicating that the energy independent, non-endocytic internalization was closely related to the species of aromatic groups. In a further step, siRNA delivery into H9C2 cells was evaluated in the presence of various endocytic inhibitors. As indicated by Fig. S3,† the cellular uptake level was significantly reduced by chlorpromazine (inhibitor for clathrin-mediated endocytosis) and wortmannin (inhibitor for macropinocytosis), while caveolae inhibitors, genistein and mβCD, showed negligible inhibitory effect. These results thus demonstrated that part of polypeptide/siRNA polyplexes were taken up by H9C2 cells *via* cla-

thrin-mediated endocytosis and macropinocytosis pathway rather than caveolae.

We have previously found that the membrane-penetrating capability of α-helical polypeptides is also related to a unique "pore formation" mechanism,[42,52,53] an effective trans-membrane delivery mechanism which however, will also cause irreversible damage to the cell membranes. As such, we further explored the pore formation abilities of the polypeptides by measuring the cellular uptake level of a membrane-impermeable dye, FITC-Tris, after co-incubation with various polypeptides. As shown in Fig. 5D, all tested polypeptides triggered dramatically higher FITC uptake level than free FITC-Tris, confirming the pore formation behavior of these helical polypeptides. However, it is noteworthy that the introduction of aromatic groups did not enhance the uptake level of FITC-Tris comparing to P-Homo, except for P-Biph and P-Pyre. Such result implied that aromatic domains did not promote or impede "pore formation" ability of helical polypeptides. Combining with the siRNA uptake level in the presence of endocytic inhibitors, the internalization way of these aromatic polypeptides, especially for P-Ben and P-Naph, might not only rely on "pore formation" mechanism, but also direct translocation pathway.

The endosomal escape of polyplexes was observed by CLSM. As shown in Fig. 5E, after treatment of H9C2 cells with P-Ben/FAM-siRNA polyplexes for 4 h, much more FAM-siRNA molecules were internalized, as indicated by the presence of green fluorescence. More importantly, the low colocalization ratio between green and red fluorescence (7.8%) indicated that internalized polyplexes underwent effective endosomal escape due to the potent membrane activities provided by aromatic domains. In comparison, the P-Homo resulted in significantly higher colocalization ratio (27.1%) even after 4 h treatment, which corresponded to high level of endosomal entrapment. These results correlated well with enhanced gene silencing efficiencies of aromatic polypeptides compared to the homopolypeptide.

In vivo cell uptake

To evaluate the siRNA delivery efficiency into cardiac cells *in vivo*, polyplexes containing Cy3-siRNA were injected into

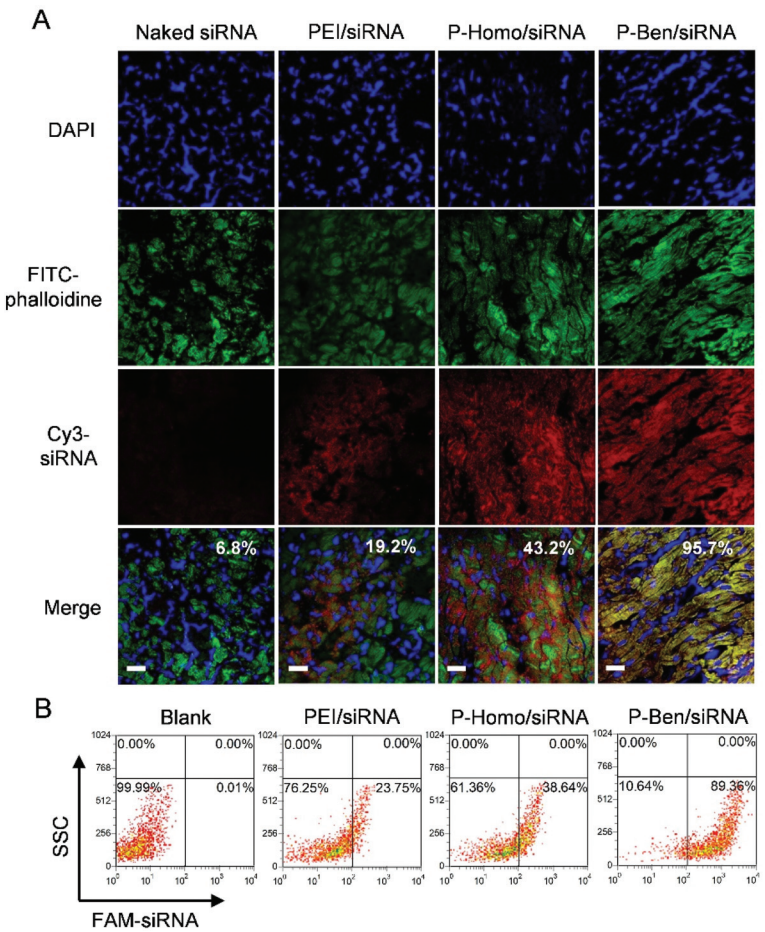

Fig. 6 *In vivo* cellular internalization of polymer/siRNA polyplex. (A) CLSM images of ischemic myocardium sections at 4 h post injection of naked Cy3-siRNA or polymer/Cy3-siRNA polyplexes (polypeptide/siRNA = 15, PEI/siRNA = 2.5, w/w). The cardiac cells were stained with FITC-phalloidine (50 μg mL^{-1}). The colocalization ratios between Cy3-siRNA and FITC-phalloidine were listed (n = 20). Scale bar = 25 μm. (B) Flow cytometric analysis on the uptake level of polyplexes containing FAM-siRNA in cardiac cells (n = 4).

myocardium followed by CLSM observation at 4 h post injection. As shown in Fig. 6A, free Cy3-siRNA was negligibly distributed in cardiac cells, due to its membrane impermeability. P-Ben, the top-performing polypeptide identified above, showed strong intracellular siRNA delivery efficiency, as evidenced by the strong red fluorescence throughout the left ventricle sections. Furthermore, P-Ben/Cy3-siRNA polyplexes displayed a significantly higher colocalization ratio (95.7%) between green fluorescence (FITC-phalloidine-stained myocardium cells) and red fluorescence (Cy3-siRNA), in comparison to P-Homo/Cy3-siRNA polyplexes (43.2%) and PEI/Cy3-siRNA polyplexes (19.2%), substantiating the superiority of the membrane-penetrating helical polypeptide in mediating *in vivo* cardiac cell uptake that was further strengthened by the aromatic modification.

To quantify the cellular uptake level, cardiac cells were subjected to flow cytometric analysis, which revealed that 89.4% of the cardiac cells had taken up the P-Ben/FAM-siRNA polyplexes, in comparison to the notably lower uptake level of P-Homo/FAM-siRNA polyplexes (38.6%) and PEI/FAM-siRNA polyplexes (23.8%) (Fig. 6B). Such result thus highlighted the potency of aromatic helical polypeptide in mediating transmembrane siRNA delivery in myocardium *in vivo*, a critical challenge against the full performance of myocardial RNAi.

In vivo RAGE silencing efficiency and anti-inflammatory effect

In accordance with the *in vitro* silencing efficiency and *in vivo* accumulation level of siRNA in cardiac cells, the RAGE mRNA level in injured heart tissues was suppressed by 84.0% after injection of P-Ben/siRAGE polyplexes, notably outperforming PEI/siRAGE polyplexes (54.5%) and P-Homo/siRAGE polyplexes (55.2%) (Fig. 7A). The expression level of RAGE protein was consistently down-regulated by P-Ben/siRAGE polyplexes, as evaluated by the western blot analysis (Fig. 7B and C). These results thus indicated that the polyplexes based on the aromatic helical polypeptide, P-Ben, were able to efficiently suppress the high level of RAGE during the inflammatory cascades after IR injury.

As previously reported, along with the up-regulation of RAGE after IR injury, tumor necrosis factor alpha (TNF-α) and interleukin-6 (IL-6), two pro-inflammatory cytokines downstream the RAGE regulation pathway, are significantly up-regulated to cascade inflammation.[54,55] As such, we further evaluated the expression levels of TNF-α and IL-6. Western blot analysis showed that the TNF-α protein level was significantly decreased after injection with P-Ben/siRAGE polyplexes (Fig. 7B and C), and immunofluorescence staining of injured myocardium further substantiated notable down-regulation of TNF-α (red fluorescence) and IL-6 (green fluorescence) (Fig. 7D). These findings thus substantiated that the P-Ben/siRAGE polyplexes effectively silenced the RAGE expression and further down-regulated pro-inflammatory cytokines to provoke anti-inflammatory effect.

Reduction of myocardial infarct size and fibrosis

Myocardial infarct size of heart tissues after treatment with different polyplexes was determined by TTC-staining (Fig. 8A).

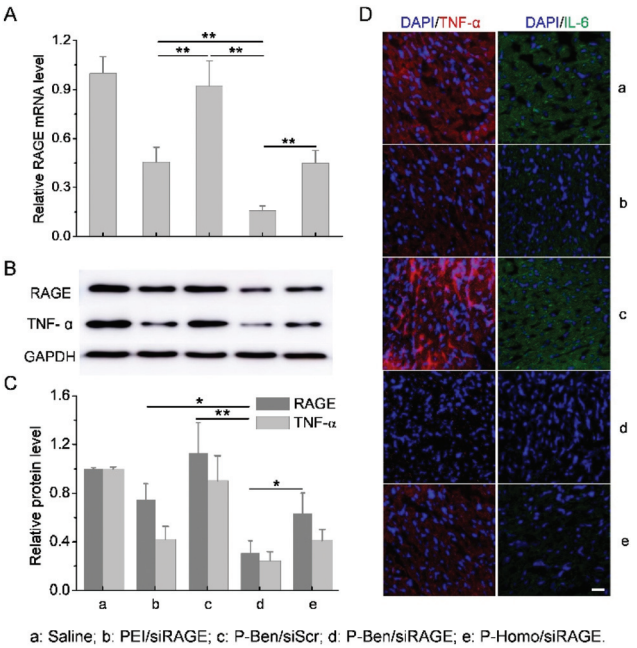

Fig. 7 Polypeptide/siRAGE polyplexes (150 μg siRNA per kg) enabled RAGE silencing and anti-inflammatory effect in rat ischemic myocardium. (A) Relative RAGE mRNA levels in ischemic myocardium at 24 h post IR injury (n = 4). (B) Western blot analysis on the RAGE and TNF-α levels in ischemic myocardium at 24 h post IR injury. (C) Quantification of the RAGE and TNF-α levels according to the western blot analysis in (B) (n = 4). (D) Representative images of myocardial sections stained for TNF-α and IL-6 at 24 h post IR injury. Scale bar = 25 μm.

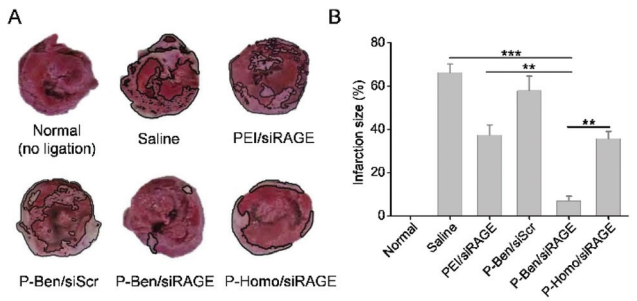

Fig. 8 Polypeptide/siRAGE polyplexes (150 μg siRNA per kg) reduced infarct size in ischemic myocardium at 1 week post IR injury. (A) Representative images of TTC-stained myocardium sections. (B) Calculated infarct size of the left ventricular myocardium (n = 4).

Consistent with the anti-inflammatory efficiency, P-Ben/siRAGE polyplexes led to remarkably reduced infarct size (white) after IR injury. The relative infarct size was represented by the order of P-Ben/siRAGE polyplexes (6.9%) < P-Homo/siRAGE polyplexes (35.7%) ≈ PEI/siRAGE polyplexes (37.3%) < P-Ben/siScr polyplexes (57.9%) ≈ saline (66.3%), which accorded well with the trend in the anti-inflammatory capabilities.

In the self-repairing process after MI injury, post-inflammatory response will cause some irreversible damages, including

cardiomyocyte death, tissue injury, and cardiac fibrosis.[4] Thus, the injury of heart tissues was first evaluated by H&E staining. As shown in Fig. 9A, rat heart displayed fiber connective tissue atrophy at 7 days post IR injury. However, rat hearts treated with P-Ben/siRAGE polyplexes showed significantly reduced tissue degeneration, as indicated by the compact arrangements of cardiac cells. Furthermore, the cardiac fibrosis of rat heart was explored by determining the presence of collagen deposition using Masson's trichrome (MT) staining. As shown in Fig. 9B, IR-injured rat heart showed massive collagen deposition (stained in blue), which was dramatically alleviated by the treatment with P-Ben/siRAGE polyplexes. In consistence with the RAGE silencing and anti-inflammatory efficiencies, P-Ben/siRAGE polyplexes outperformed P-Homo/siRNA polyplexes and PEI/siRAGE polyplexes in terms of the calculated fibrosis area (fibrotic area normalized by the total cross-sectional area) in the following order of P-Ben/siRAGE polyplexes (11.8%) < PEI/siRAGE polyplexes (38.7%) ≈ P-Homo/siRAGE polyplexes (34.2%) < P-Ben/siScr polyplexes (66.6%) ≈ control (PBS, 66.0%) (Fig. 9D).

These results collectively demonstrated that the P-Ben/siRAGE polyplexes could substantially reduce cardiac IR injury through reduction of infarct size and cardiac fibrosis, as a consequence of the effective knockdown of inflammatory factors in cardiac cells.

Anti-apoptotic effect

During post-infarct cardiac remodeling, IR injury will accelerate the apoptosis of cardiomyocytes. Thus, the anti-apoptotic effect of siRAGE delivery was investigated using the TUNEL assay. The apoptotic cells appeared brown color under optical microscope, while normal cells were stained blue (Fig. 9C).

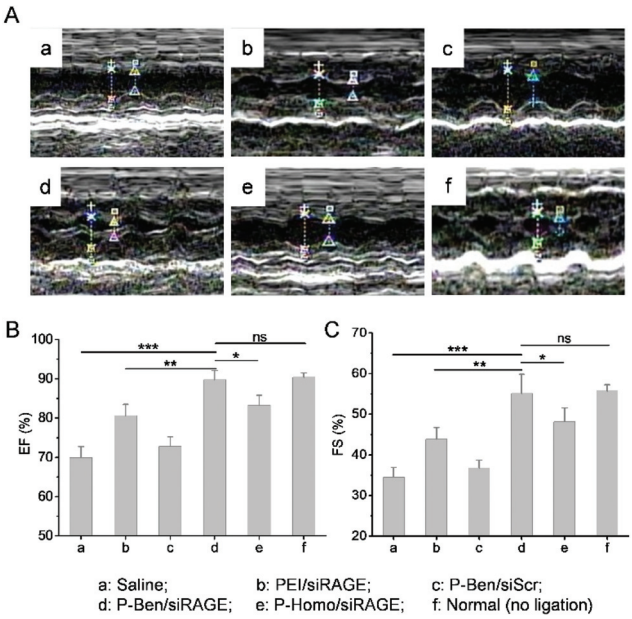

Fig. 10 Polypeptide/siRAGE polyplexes (150 μg siRNA per kg) recovered cardiac function at 3 days post IR injury. (A) Echocardiographic graphs of rats after different polyplexes treatment. (B) Ejection fraction (EF, %) and (C) fraction shortening (FS, %) of the left ventricule as indicated by echocardiography (n = 4).

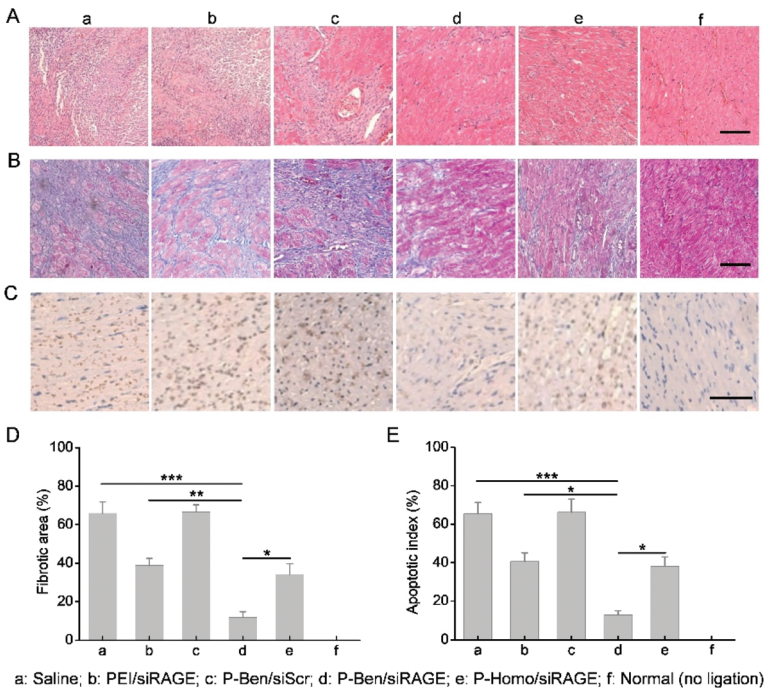

Fig. 9 Polypeptide/siRAGE polyplexes (150 μg siRNA per kg) alleviated apoptosis, necrosis, and fibrosis in rat ischemic myocardium at 1 week post IR injury. Representative images of myocardium sections following HE staining (A), MT staining (B), and TUNEL staining (C). Scale bar = 200 μm. Calculated fibrotic area (D) and apoptosis ratio (E) from MT- and TUNEL-stained myocardium sections, respectively (n = 4).

The apoptotic cells in cardiac tissues treated with P-Ben/siRAGE polyplexes (12.9%) were effectively decreased at 7 days post IR injury, significantly lower than those detected for P-Homo/siRAGE polyplexes (38.2%) and PEI/siRAGE polyplexes (40.6%).

siRAGE-mediated recovery of cardiac function

The cardiac function was measured by echocardiography three days after IR injury. As showed in Fig. 10A, MI can be illustrated by the presence of prolonged long-axis shortening (post-ejection shortening, right-side arrow).[56] Less conspicuous changes in the left ventricle (LV) function and a smaller ventricular expansion were noted in rat hearts treated with P-Ben/siRAGE polyplexes. Furthermore, left ventricular ejection fraction (EF) and fractional shortening (FS), two important parameters related to the left ventricular function of rat hearts, were determined. The EF and FS values of rat hearts treated with P-Ben/siRAGE polyplexes were significantly higher than other tested polyplexes, and they almost recovered to the normal values (Fig. 10B and C). Such results thus indicated that P-Ben/siRAGE polyplexes could significantly attenuate cardiac remodeling and fully recover the cardiac function, as a consequence of their potent anti-inflammatory capability.

Conclusions

In this study, we developed guanidinated helical polypeptides with potent and aromaticity-assisted membrane activities to mediate anti-inflammatory siRAGE delivery against myocardial IR injury. Ben-modified polypeptide (P-Ben) was identified as the best-performing material with the strongest membrane activity, highest gene knockdown efficiency, and lowest cytotoxicity in H9C2 cells. Thus, after intracardial injection, the P-Ben/siRAGE polyplexes allowed efficient transcellular delivery into the cardiomyocytes to provoke remarkable RAGE silencing, which consequently suppressed myocardial inflammation, apoptosis, and fibrosis to recover the cardiac function after IR injury. This study therefore provides an effective approach to tailor the membrane penetration capability of siRNA delivery materials, and it also renders a promising modality for the treatment of myocardial IR injury.

Conflicts of interest

There are no conflicts to declare.

Acknowledgements

We acknowledge the financial support from the Ministry of Science and Technology of China (2016YFA0201200), the National Natural Science Foundation of China (51722305, 51573123, and 51873142), 111 project, and Priority Academic Program Development of Jiangsu Higher Education Institutions (PAPD).

References

1 P. Dutta, G. Courties, Y. Wei, F. Leuschner, R. Gorbatov, C. S. Robbins, Y. Iwamoto, B. Thompson, A. L. Carlson, T. Heidt, M. D. Majmudar, F. Lasitschka, M. Etzrodt, P. Waterman, M. T. Waring, A. T. Chicoine, A. M. van der Laan, H. W. M. Niessen, J. J. Piek, B. B. Rubin, J. Butany, J. R. Stone, H. A. Katus, S. A. Murphy, D. A. Morrow, M. S. Sabatine, C. Vinegoni, M. A. Moskowitz, M. J. Pittet, P. Libby, C. P. Lin, F. K. Swirski, R. Weissleder and M. Nahrendorf, *Nature*, 2012, **487**, 325–329.
2 A. E. Moran, M. H. Forouzanfar, G. A. Roth, G. A. Mensah, M. Ezzati, A. Flaxman, C. J. L. Murray and M. Naghavi, *Circulation*, 2014, **129**, 1493–1501.
3 A. Moorthi, Y.-C. Tyan and T.-W. Chung, *Biomater. Sci.*, 2017, **5**, 1976–1987.
4 N. G. Frangogiannis, *Circ. Res.*, 2012, **110**, 159–173.
5 T. J. Cahill, R. P. Choudhury and P. R. Riley, *Nat. Rev. Drug Discovery*, 2017, **16**, 699–717.
6 A. Kaczmarek, P. Vandenabeele and D. V. Krysko, *Immunity*, 2013, **38**, 209–223.
7 N. G. Frangogiannis, *Nat. Rev. Cardiol.*, 2014, **11**, 255–265.
8 G. Heusch, *Circ. Res.*, 2015, **116**, 674–699.
9 S. D. Prabhu and N. G. Frangogiannis, *Circ. Res.*, 2016, **119**, 91–112.
10 P. Libby, *Nature*, 2002, **420**, 868–874.
11 E. H. Kobayashi, T. Suzuki, R. Funayama, T. Nagashima, M. Hayashi, H. Sekine, N. Tanaka, T. Moriguchi, H. Motohashi, K. Nakayama and M. Yamamoto, *Nat. Commun.*, 2016, **7**, 14.
12 C. A. Dinarello, *Blood*, 2011, **117**, 3720–3732.
13 C. Shi, Y. Zhao, Y. Yang, C. Chen, X. Hou, J. Shao, H. Yao, Q. Li, Y. Xia and J. Dai, *Biomater. Sci.*, 2018, **6**, 356–363.
14 S. Steffens, F. Montecucco and F. Mach, *Thromb. Haemostasis*, 2009, **102**, 240–247.
15 M. S. Ji, M. H. Jeong, Y. k. Ahn, S. H. Kim, Y. J. Kim, S. C. Chae, T. J. Hong, I. W. Seong, J. K. Chae, C. J. Kim, M. C. Cho, S.-W. Rha, J. H. Bae, K. B. Seung and S. J. Park, *Int. J. Cardiol.*, 2016, **225**, 50–59.
16 Y. Jiang, J. W. Bai, L. X. Tang, P. Zhang and J. Pu, *Cell. Physiol. Biochem.*, 2015, **37**, 979–990.
17 C. A. Dinarello, A. Simon and J. W. M. van der Meer, *Nat. Rev. Drug Discovery*, 2012, **11**, 633–652.
18 J. Haasnoot, E. M. Westerhout and B. Berkhout, *Nat. Biotechnol.*, 2007, **25**, 1435–1443.
19 B. L. Davidson and P. B. McCray, *Nat. Rev. Genet.*, 2011, **12**, 329–340.
20 L. Zhang, W. Zheng, R. Tang, N. Wang, W. Zhang and X. Jiang, *Biomaterials*, 2016, **104**, 269–278.
21 J. J. Rossi, C. H. June and D. B. Kohn, *Nat. Biotechnol.*, 2007, **25**, 1444–1454.
22 M. Aouadi, G. J. Tesz, S. M. Nicoloro, M. X. Wang, M. Chouinard, E. Soto, G. R. Ostroff and M. P. Czech, *Nature*, 2009, **458**, 1180–U1116.
23 W. Zhang, Y. Zhou, X. Li, X. Xu, Y. Chen, R. Zhu and L. Yin, *Biomater. Sci.*, 2018, **6**, 1986–1993.

24 W. Liao, W. Li, T. Zhang, M. Kirberger, J. Liu, P. Wang, W. Chen and Y. Wang, *Biomater. Sci.*, 2016, **4**, 1051–1061.
25 M. Dimde, F. Neumann, F. Reisbeck, S. Ehrmann, J. L. Cuellar-Camacho, D. Steinhilber, N. Ma and R. Haag, *Biomater. Sci.*, 2017, **5**, 2328–2336.
26 L. C. Yin, H. Y. Tang, K. H. Kim, N. Zheng, Z. Y. Song, N. P. Gabrielson, H. Lu and J. J. Cheng, *Angew. Chem., Int. Ed.*, 2013, **52**, 9182–9186.
27 J. Hong, S. H. Ku, M. S. Lee, J. H. Jeong, H. Mok, D. Choi and S. H. Kim, *Biomaterials*, 2014, **35**, 7562–7573.
28 M. Dobaczewski, W. Chen and N. G. Frangogiannis, *J. Mol. Cell. Cardiol.*, 2011, **51**, 600–606.
29 M. Andrassy, H. C. Volz, J. C. Igwe, B. Funke, S. N. Eichberger, Z. Kaya, S. Buss, F. Autschbach, S. T. Pleger, I. K. Lukic, F. Bea, S. E. Hardt, P. M. Humpert, M. E. Bianchi, H. Mairbaurl, P. P. Nawroth, A. Remppis, H. A. Katus and A. Bierhaus, *Circulation*, 2008, **117**, 3216–3226.
30 H. Yanai, T. Ban, Z. Wang, M. K. Choi, T. Kawamura, H. Negishi, M. Nakasato, Y. Lu, S. Hangai, R. Koshiba, D. Savitsky, L. Ronfani, S. Akira, M. E. Bianchi, K. Honda, T. Tamura, T. Kodama and T. Taniguchi, *Nature*, 2009, **462**, 99–110.
31 C. Ott, K. Jacobs, E. Haucke, A. Navarrete Santos, T. Grune and A. Simm, *Redox Biol.*, 2014, **2**, 411–429.
32 G. P. Sims, D. C. Rowe, S. T. Rietdijk, R. Herbst and A. J. Coyle, *Annu. Rev. Immunol.*, 2010, **28**, 367–388.
33 E. Harja, D. X. Bu, B. I. Hudson, J. S. Chang, X. P. Shen, K. Hallam, A. Z. Kalea, Y. Lu, R. H. Rosario, S. Oruganti, Z. Nikolla, D. Belov, E. Lalla, R. Ramasamy, S. F. Yan and A. M. Schmidt, *J. Clin. Invest.*, 2008, **118**, 183–194.
34 L. G. Bucciarelli, M. Kaneko, R. Ananthakrishnan, E. Harja, L. K. Lee, Y. C. Hwang, S. Lerner, S. Bakr, Q. Li, Y. Lu, F. Song, W. Qu, T. Gomez, Y. S. Zou, S. F. Yan, A. M. Schmidt and R. Ramasamy, *Circulation*, 2006, **113**, 1226–1234.
35 M. Morille, C. Passirani, A. Vonarbourg, A. Clavreul and J. P. Benoit, *Biomaterials*, 2008, **29**, 3477–3496.
36 S. R. Mao, W. Sun and T. Kissel, *Adv. Drug Delivery Rev.*, 2010, **62**, 12–27.
37 S. Suarez, A. Almutairi and K. L. Christman, *Biomater. Sci.*, 2015, **3**, 564–580.
38 Y. Li, B. Humphries, Z. Wang, S. Lang, X. Huang, H. Xiao, Y. Jiang and C. Yang, *ACS Appl. Mater. Interfaces*, 2016, **8**, 30735–30746.
39 Y. C. Chen, D. Y. Gao and L. Huang, *Adv. Drug Delivery Rev.*, 2015, **81**, 128–141.
40 V. Gupta and K. D. Poss, *Nature*, 2012, **484**, 479–U102.
41 Q. L. Lu, G. Bou-Gharios and T. A. Partridge, *Gene Ther.*, 2003, **10**, 131.
42 L. Yin, Z. Song, K. H. Kim, N. Zheng, N. P. Gabrielson and J. Cheng, *Adv. Mater.*, 2013, **25**, 3063–3070.
43 N. P. Gabrielson, H. Lu, L. Yin, D. Li, F. Wang and J. Cheng, *Angew. Chem., Int. Ed.*, 2012, **51**, 1143–1147.
44 L. Yin, Z. Song, K. H. Kim, N. Zheng, H. Tang, H. Lu, N. Gabrielson and J. Cheng, *Biomaterials*, 2013, **34**, 2340–2349.
45 M. H. Turabee, T. Thambi, H. T. T. Duong, J. H. Jeong and D. S. Lee, *Biomater. Sci.*, 2018, **6**, 661–671.
46 Z. Guo, X. Zhou, M. Xu, H. Tian, X. Chen and M. Chen, *Biomater. Sci.*, 2017, **5**, 2501–2510.
47 G. Lättig-Tünnemann, M. Prinz, D. Hoffmann, J. Behlke, C. Palm-Apergi, I. Morano, H. D. Herce and M. C. Cardoso, *Nat. Commun.*, 2011, **2**, 453.
48 Y. G. Huang, Y. H. Zeng, J. W. Yang, Z. H. Zeng, F. M. Zhu and X. D. Chen, *Chem. Commun.*, 2011, **47**, 7509–7511.
49 A. H. Cohen, *Am. J. Clin. Pathol.*, 1976, **65**, 631–643.
50 H. Lu and J. J. Cheng, *J. Am. Chem. Soc.*, 2007, **129**, 14114–14115.
51 Q. Yin, R. Tong, L. C. Yin, T. M. Fan and J. J. Cheng, *Polym. Chem.*, 2014, **5**, 1581–1585.
52 R. Zhang, N. Zheng, Z. Song, L. Yin and J. Cheng, *Biomaterials*, 2014, **35**, 3443–3454.
53 F. Li, Y. Li, Z. Zhou, S. Lv, Q. Deng, X. Xu and L. Yin, *ACS Appl. Mater. Interfaces*, 2017, **9**, 23586–23601.
54 S. Zeng, H. Dun, N. Ippagunta, R. Rosario, Q. Y. Zhang, J. Lefkowitch, S. F. Yang, A. M. Schmidt and J. C. Emond, *J. Hepatol.*, 2009, **50**, 929–936.
55 D. Brenner, H. Blaser and T. W. Mak, *Nat. Rev. Immunol.*, 2015, **15**, 362–374.
56 S. Price, E. Platz, L. Cullen, G. Tavazzi, M. Christ, M. R. Cowie, A. S. Maisel, J. Masip, O. Miro, J. J. McMurray, W. F. Peacock, F. J. Martin-Sanchez, S. Di Somma, H. Bueno, U. Zeymer, C. Mueller and A. for the Acute Heart Failure Study Group of the European Society of Cardiology Acute Cardiovascular Care, *Nat. Rev. Cardiol.*, 2017, **14**, 427–440.

